ADVANCED HEALTHCARE MATERIALS
www.advhealthmat.de

Development of 3D Printed Biodegradable, Entirely X-ray Visible Stents for Rabbit Carotid Artery Implantation

Yihong Shen, Chaojie Tang, Binbin Sun, Yufan Wu, Xiao Yu, Jie Cui, Mianmian Zhang, Mohamed EL-Newehy, Hany EL-Hamshary, Peter Barlis, Wu Wang, and Xiumei Mo**

Biodegradable stents are considered a promising strategy for the endovascular treatment of cerebrovascular diseases. The visualization of biodegradable stents is of significance during the implantation and long-term follow-up. Endowing biodegradable stents with X-ray radiopacity can overcome the weakness of intrinsic radioparency of polymers. Hence, this work focuses on the development of an entirely X-ray visible biodegradable stent (PCL-KIO_3) composed of polycaprolactone (PCL) and potassium iodate via physical blending and 3D printing. The in vitro results show that the introduction of potassium iodate makes the 3D-printed PCL stents visualizable under X-ray. So far, there is inadequate study about polymeric stent visualization in vivo. Therefore, PCL-KIO_3 stents are implanted into the rabbit carotid artery to evaluate the biosafety and visibility performance. During stent deployment, the visualization of the PCL-KIO_3 stent effectively helps to understand the position and dilation status of stents. At 6-month follow-up, the PCL-KIO_3 stent could still be observed under X-ray and maintains excellent vessel patency. To sum up, this study demonstrates that PCL-KIO_3 stent may provide a robust strategy for biodegradable stent visualization.

1. Introduction

Cerebrovascular disease, as a circulation system disease, has become one of the leading threats to public health.[1] The carotid artery is one of the major supply routes of blood strain to the brain. When intracranial vascular stenosis or occlusion occurs, the brain cannot be supplied with sufficient blood, thus resulting in the occurrence of cerebral ischemic stroke. In the clinic, the implantation of a vascular stent in the diseased carotid artery is an effective way of supporting stenotic or occluded vessels and restoring blood flow to the brain.[2] At present, endovascular treatment (EVT) with drug-eluting stents is in common use in clinics because it can greatly reduce the incidence of restenosis of targeted blood vessels. However, these stents are usually made of non-degradable metals. The permanent presence in the body is likely to lead to the occurrences of late thrombosis, very late thrombosis, and other adverse events. Therefore, the emergence of biodegradable stents provides a new therapeutic means for treating cerebrovascular diseases.[3–5] At the early stage of implantation, the biodegradable stents play the role of supporting diseased cerebral vessels. After the vessel has been restored to a healthy state, the stent gradually degraded into small molecules. The last decade has witnessed rapid progress in cardiovascular and cerebrovascular medical devices.[6,7] While biodegradable stents have been extensively investigated,[8,9] the X-ray radiopaque and biodegradable materials are so

Y. Shen, B. Sun, X. Yu, J. Cui, X. Mo
State Key Laboratory for Modification of Chemical Fibers and Polymer Materials
Shanghai Engineering Research Center of Nano-Biomaterials and Regenerative Medicine
College of Biological Science and Medical Engineering
Donghua University
Shanghai 201620, P. R. China
E-mail: xmm@dhu.edu.cn

C. Tang, W. Wang
Department of Radiology
Longhua Hospital
Shanghai University of Traditional Chinese Medicine
Shanghai 200032, China
E-mail: wangwangwuwu@hotmail.com

C. Tang, Y. Wu, M. Zhang, W. Wang
Institute of Diagnostic and Interventional Radiology
Shanghai Jiao Tong University Affiliated Sixth People's Hospital
Shanghai 200233, P. R. China

M. EL-Newehy, H. EL-Hamshary
Department of Chemistry
College of Science
King Saud University
P.O. Box 2455, Riyadh 11451, Saudi Arabia

P. Barlis
Department of Medicine
Melbourne Medical School
Faculty of Medicine
Dentistry & Health Sciences
The University of Melbourne
Parkville, VIC 3010, Australia

The ORCID identification number(s) for the author(s) of this article can be found under https://doi.org/10.1002/adhm.202304293

DOI: 10.1002/adhm.202304293

far very limited, which hinders their clinical applications. The present study is aimed at developing a new biodegradable and X-ray visible polymer to fabricate cerebrovascular stents.

Conferring the radiopacity property onto polymer materials similar to metal stents is of great significance for stent visualization. During the deployment of stents, excessive dilation of stents may cause damage to blood vessels and even vascular rupture.[10] On the contrary, insufficient stent dilation may lead to incomplete apposition and asymmetric dilation, resulting in an increased risk of thrombosis.[11] In an attempt to overcome these issues, the evaluation of the real-time status of biodegradable stents via non-invasive imaging technology is considered an effective method to improve the success rate of implantation.[12] However, most of the biodegradable polymeric stents are composed of C, O, H, and N. They are elements with low specific gravity and low electron density. On account of the similarity to elements of the human body, most biodegradable polymeric stents exhibit a lack of radiopacity and poor contrast, so that they cannot be observed under X-ray. X-ray visualization of biodegradable stents enables clinicians to understand the position and status of stents during implantation, which can avoid clinical adverse events in relation to the inability to access, deploy, or withdraw. Moreover, due to the non-invasiveness of X-rays, the morphological changes and structural integrity of biodegradable stents can be evaluated under X-ray during follow-up, avoiding other traumatic examinations and reducing the risk of postoperative complications. Currently, the immobilization of radiopaque markers at the distal and proximal end is one of the major methods for the visualization of polymeric stents.[13,14] The metallic markers, such as platinum, tantalum, and gold, can be immobilized at the end of the stent for deployment. Nevertheless, these markers can merely display the position of the stent and fail to fully show the stent dilation and structural morphology. The status of the stent is incapable of being evaluated by clinicians during the intraoperation and post-operation, which brings about surgical difficulties.[15] Moreover, these markers will remain in the body for a lifetime, resulting in great concern about the potential risk. Based on the above limitations, the development of entirely X-ray visible biodegradable stents has aroused widespread attention.

In order to solve the problem of invisibility of bulk polymer materials, it may be effective to introduce some contrast agents into the polymer to realize the visualization of the stent. So far, various strategies have been executed for entirely stent visualization such as physical blend and chemical modification.[16–19] In terms of chemical modification, in spite of the increased radiopacity of the polymer via chemical methods, the complex preparation process and potential toxicity in chemical synthesis hinder its clinical application in interventional medical devices.[20] In comparison, the combination of contrast agent and polymer matrix has been considered as a robust method for polymeric stent visualization. X-ray contrast agents, such as barium sulfate,[21] zirconia,[22] and iron oxide,[23] can be blended with polymer materials to prepare a radiopaque polymer composite. However, barium sulfate and other barium agents are widely used in gastrointestinal imaging,[24] and the biosafety of its application in the cerebrovascular system is of great concern.[25] The potential toxicity of these heavy metallic contrast agents should not be ignored. In addition, most of the current studies of X-ray visible stents are still limited to in vitro experiments. Due to the increased background radiopacity resulting from bones and muscles, the visibility of X-ray visible stent in vivo is lower than that of in the air, which limits its clinical application. Therefore, it is still a severe challenge to improve the radiopacity and biosafety of stents in vivo.

The goal of this work is to develop an entirely X-ray visible biodegradable stent for cerebrovascular application. As a common X-ray contrast agent, iodinated contrast agents have extensive use in angiography. Because of the high electron density of iodine atoms, the iodine-containing compound potassium iodate (KIO_3) possesses excellent X-ray absorption properties.[26] Therefore, we developed a kind of radiopaque 3D printed ink by blending potassium iodate with polycaprolactone (PCL). Then we used the radiopaque ink according to a specific computer model to prepare an entirely X-ray visible stent (PCL-KIO_3 stent). The X-ray imaging performance in vitro of the stents was evaluated. Afterward, the stent was implanted into the rabbit's carotid artery. After 6 months of implantation, the X-ray imaging capacity in vivo and biocompatibility of the entirely X-ray visible stent were evaluated (**Figure 1**).

2. Results

2.1. Characterization of Stents

In order to prepare X-ray visible stents, PCL and KIO_3 were dissolved in a dichloromethane (DCM) solution. Then the PCL-KIO_3 composites were dried in a vacuum to obtain PCL-KIO_3 3D printed ink. With the increase in temperature, the PCL-KIO_3 printed ink became a molten state. The uniform fusant was received on stainless steel rods by a four-axis printing system (**Figure 2A**). In terms of digital photos, both PCL and PCL-KIO_3 stents can maintain their original shape after being stripped from the steel rod (Figure 2B). The basic parameter of the samples was shown (Table S1, Supporting Information). Scanning electron microscope (SEM) images demonstrated that the fibers of PCL and PCL-KIO_3 stents were well organized. The upper and lower layers of fibers were firmly combined to form a stable structure. The surface of PCL fiber was smooth, while the surface of PCL-KIO_3 fiber was relatively rough. The singular KIO_3 particle was either completely embedded in the stent fiber or attached to the surface of the stent strut (Figure 2C). The energy dispersive spectrometer (EDS) element mapping image (Figure 2D) showed the distribution of carbon, oxygen, potassium, and iodine in the PCL-KIO_3 stent. In theory, the elements of carbon and oxygen existed in PCL. The distribution of iodine and potassium on the PCL-KIO_3 stent confirmed the successful introduction of potassium iodate.

The X-ray diffraction (XRD) patterns of the PCL-KIO_3 stents and KIO_3 powder are displayed in Figure S2A, Supporting Information. The characteristic diffraction peaks with high intensity at $2\theta = 19.9°$, $2\theta = 28.2°$, $2\theta = 40.3°$, $2\theta = 45.9°$, and $2\theta = 50.2°$ were observed on the diffraction pattern of the potassium iodate powder. The result of XRD patterns showed that a characteristic diffraction peak corresponding to pure KIO_3 was detected on the PCL-KIO_3 stents, demonstrating that potassium iodate existed

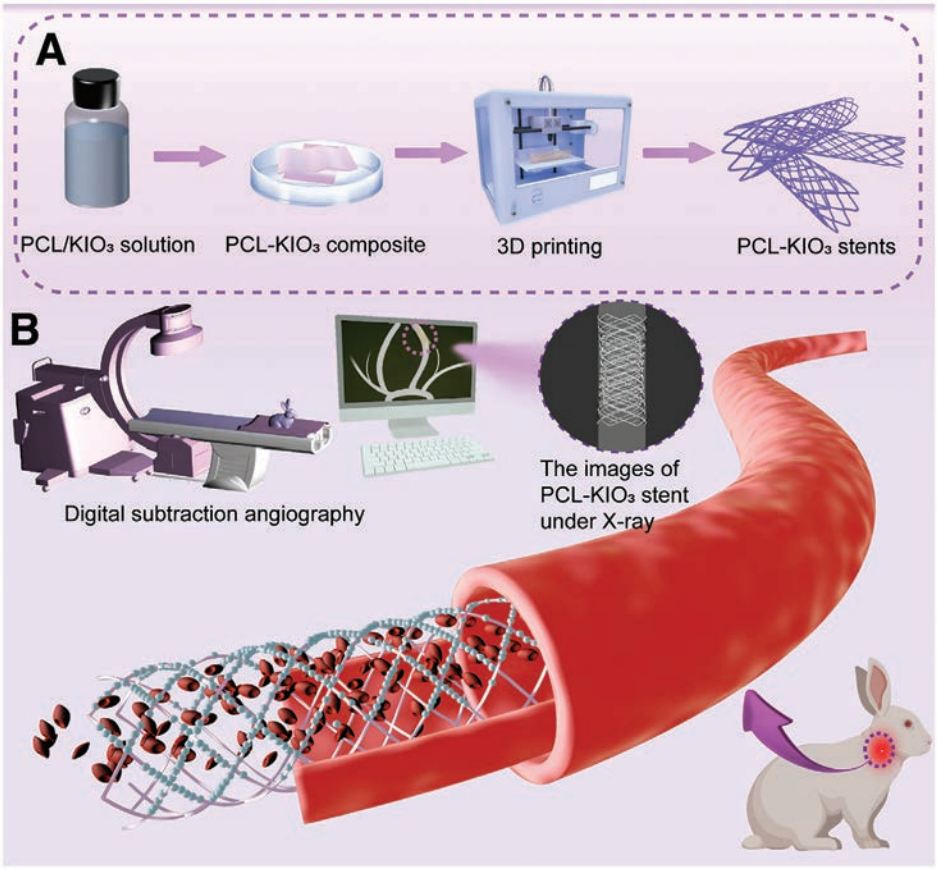

Figure 1. A) The process of preparation of PCL-KIO_3 stent. B) Schematic illustration of 3D printed biodegradable, entirely X-ray visible stents for rabbit carotid artery implantation.

amorphously in the X-ray visible stents. The thermogravimetric analysis was also used to distinguish the stent changes after embedding KIO_3. According to Figure S2B, Supporting Information, PCL, KIO_3, and their composites exhibited excellent thermal stability, with the degradation temperature far higher than 160–165 °C (the temperature used for preparing X-ray visible biodegradable stents via 3D printing), which proved that the PCL-KIO_3 printed ink was stable in the process of fabrication. According to Figure S2C, Supporting Information, the KIO_3 release kinetics obtained for the time points evaluated were depicted. In the first 4 days, the cumulative release of KIO_3 from PCL-KIO_3-100 was 21.78%, from PCL-KIO_3-150 was 25.14%, and from PCL-KIO_3-200 was 29.77%. The surface-absorbed KIO_3 contributed to the relatively rapid release. Afterward, the release was followed by a constant stable release period for the subsequent 24 days in which the cumulative release of PCL-KIO_3-100 was 26.89%, from PCL-KIO_3-150 was 29.81%, and from PCL-KIO_3-200 was 36.12%. In addition, the hydrophilicity of the stent was determined by contact angle test (Figure S2D, Supporting Information). The mean contact angle was in the range of 90.4°–94.7° and showed hydrophobicity. The loading of KIO_3 would not change the hydrophilicity of the PCL stents. The roughness of the strut surface of all stents is displayed in Figure S2E, Supporting Information, demonstrating that the surface of the PCL stents was smoother than PCL-KIO_3 stents. These observations indicated that the introduction of KIO_3 may result in the stent on rougher surfaces.

2.2. Mechanical Properties

As far as the application of vascular stents is concerned, the mechanical properties are one of the important considerations. The radial compression stress of the stent is shown in **Figure 3**A. The compression stress of the PCL stent was 0.835 ± 0.02 MPa. The compression stresses of PCL-KIO_3-100, PCL-KIO_3-150, and PCL-KIO_3-200 stents were 1.26 ± 0.11, 1.22 ± 0.06, and 1.31 ± 0.11 MPa, respectively. The addition of the rigid fillers had an effect on the mechanical reinforcement. Figure 3B presents the results of compressive modulus. The compression modulus of the PCL stent was 1.85 ± 0.11 MPa. The compression modulus of PCL-KIO_3-100, PCL-KIO_3-150, and PCL-KIO_3-200 stent was 2.19 ± 0.61, 2.64 ± 0.37, and 3.07 ± 0.26 MPa, respectively. As shown in Figure 3C, the representative stress–strain curves of the stents were presented. After ten times cyclic compression tests, the structure of PCL, PCL-KIO_3-100, PCL-KIO_3-150, and PCL-KIO_3-200 stents remained stable. Moreover, the three-point bending test was analyzed taking into account the bending resistance properties (Figure 3D). After the test, all groups could return to their original shape.

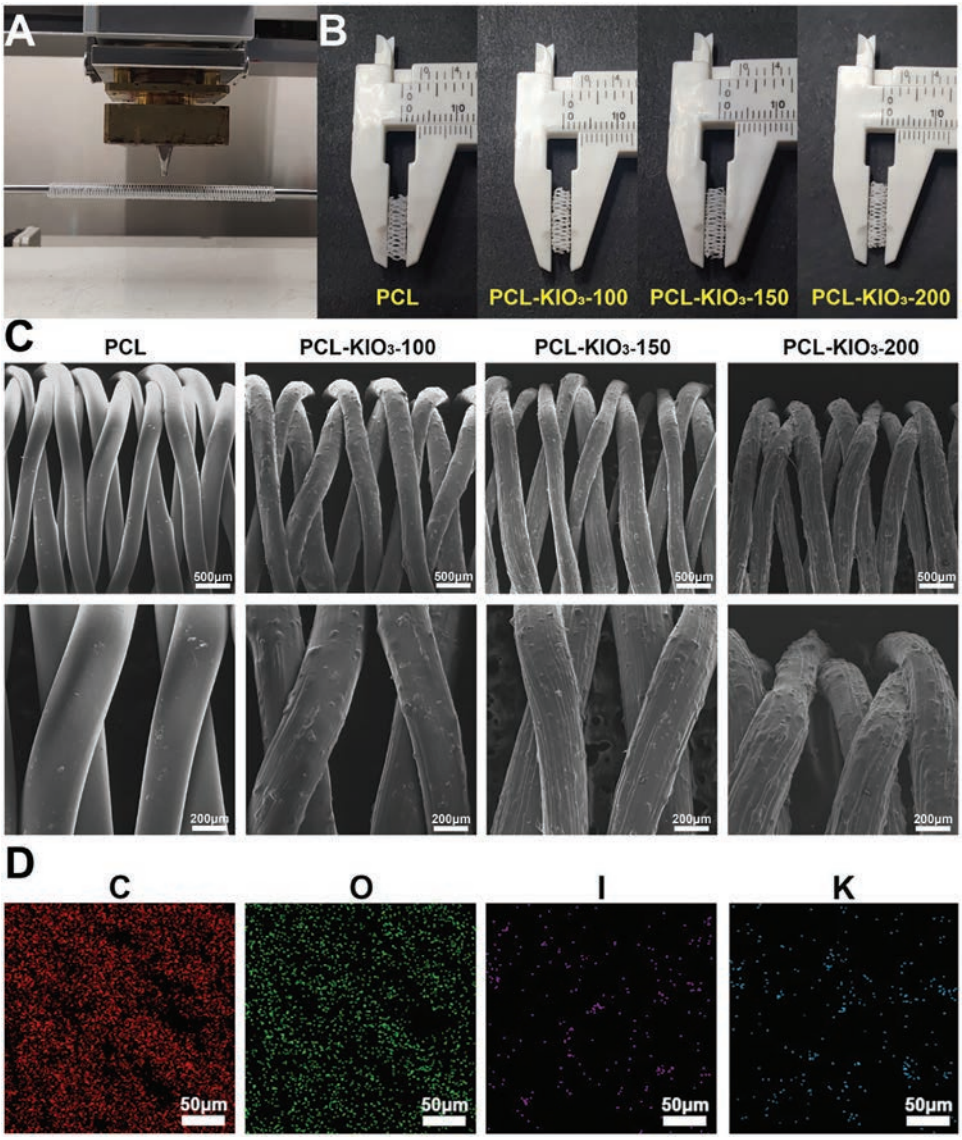

Figure 2. A) Fabrication and construction of entirely X-ray visible stents via 3D printing. B) Digital photos of PCL and PCL-KIO_3 stents. C) SEM micrographs of stents. D) The EDS element mapping of PCL-KIO_3-150 stent.

2.3. In Vitro X-ray Radiopacity of the Stent

The in vitro radiopacity of the stent under X-ray is shown in **Figure** 4A. On account of PCL is mainly composed of C, H, and O, the skeleton and morphology of the PCL stent cannot be observed under X-ray and is barely visible. The addition of potassium iodate endowed the polymeric stents with radiopacity. In the perspective mode, the visualization of PCL-KIO_3 stents was also confirmed, which can greatly help to track and guide the delivery and employment of stents during surgery (Figure 4A). For quantitative analysis, the Hounsfield unit (HU) value was used to calculate the radiation intensity of the samples (Figure 4B). With the increase in potassium iodate content, the HU value of the stents also increased. The radiopacity value could be controlled by varying the KIO_3 concentration in the 3D-printed ink.

In order to evaluate the imaging performance of the biodegradable X-ray visible stent in deep tissue, some pieces of lean pork were placed on the stent to simulate the application in vivo. Figure 4C demonstrates that the polymeric biodegradable stents can be clearly tracked at the pork thickness of 1 cm. Even though the pork thickness reached 3 cm, the outline of the stent could still be observed under X-ray, which provided the possibility for the in vivo experiment of X-ray visible stents.

2.4. In Vitro Degradation of the Stent

The mass change of PCL and PCL-KIO_3 stents after the 3- and 6-month degradation periods in phosphate-buffered saline (PBS) solution are shown in **Figure** 5A. It is worth noting that the mass loss of PCL stents was about 0.37% at the time point of 6 months.

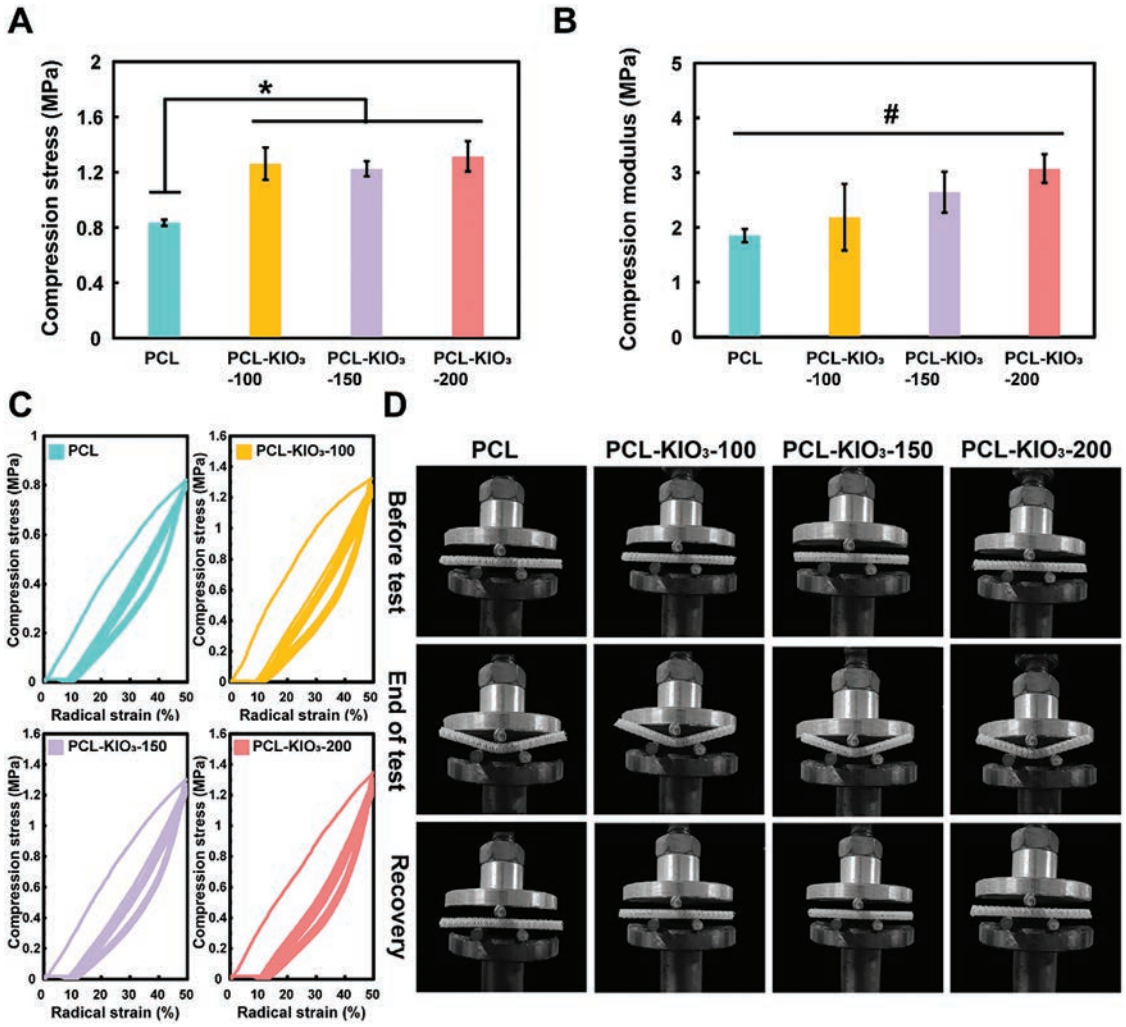

Figure 3. In vitro mechanical properties. A) Compression stress and B) compression modulus of PCL, PCL-KIO_3-100, PCL-KIO_3-150, and PCL-KIO_3-200 stents, when radially compressed to half the initial diameters. C) Typical compression load-displacement curves of stents when they were cyclically compressed for ten times. D) Images of three-point bending tests. The statistical analysis is performed by the one-way analysis of variance of Tukey's post-hoc test, $n = 3$, and $*$ indicates a significant difference of $p < 0.05$. # indicates no significant difference of $p > 0.05$.

While the mass of PCL-KIO_3-100, PCL-KIO_3-150, and PCL-KIO_3-200 stents decreased by about 5.02%, 6.26%, and 8.73%, respectively. Figure 5B demonstrates the X-ray radiopacity of the stents after degradation. After 3 months, all the X-ray visible stents can still be observed. PCL-KIO_3-150 and PCL-KIO_3-200 stents remained visible after 6 months. Figure 5C shows that the mean values of Hounsfield units of PCL-KIO_3-100, PCL-KIO_3-150, and PCL-KIO_3-200 stents decreased by 38.3%, 47.17%, and 53.09%, respectively, for 6 months. Figure S1, Supporting Information, demonstrates that the overall structures of the stent were still intact and remained unchanged after the degradation test.

2.5. Blood Compatibility of the Stent

Blood contact is inevitable for the application of vascular stents. Red blood cell hemolysis is one of the important indexes of blood compatibility of materials. As shown in Figure S3A, Supporting Information, all stents show satisfactory blood compatibility. The hemolytic ratio of PCL and PCL-KIO_3 stents was about 0.5%, indicating that the introduction of potassium iodate would not affect the hemolytic properties of the stents and meets the ISO10993-4 standard for biomaterials in contact with blood (5%).

Platelet adhesion is crucial to arterial thrombosis. As shown in Figure S3B, Supporting Information, a similar number of platelets were observed on each of the samples. Compared with PCL stent, the introduction of potassium iodate would not stimulate more platelet adhesion.

2.6. Cytocompatibility of the Stent

The design of vascular stents must minimize the adverse effects on endothelial cell proliferation and attachment. Human umbilical vein endothelial cells (HUVECs) were selected to evaluate the cytocompatibility of X-ray visible stents. The cells were seeded

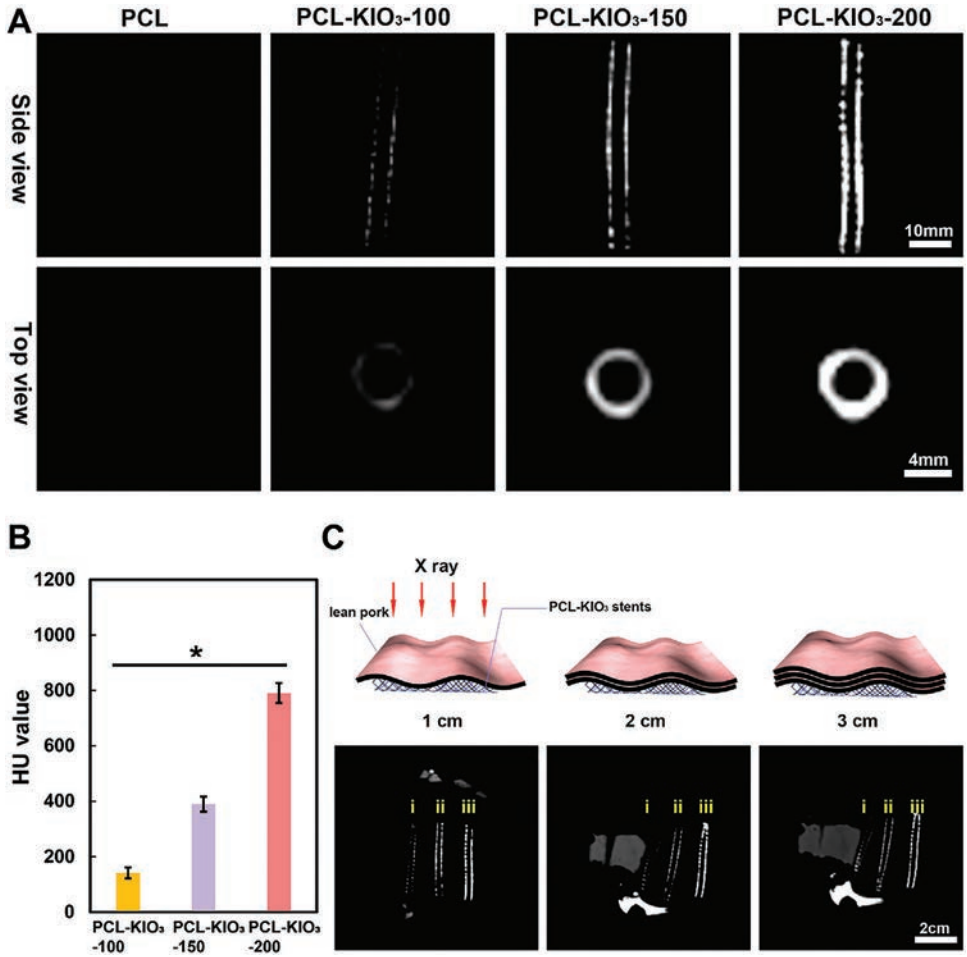

Figure 4. A) Representative radiographic images of PCL and PCL-KIO_3 stent which were placed in the air. B) X-ray attenuation of intensity in Hounsfield units (HU) of the PCL-KIO_3 stents at different concentrations in vitro. C) Representative radiographic images of PCL-KIO_3 stent which were placed inside the different diameters of lean pork (i, ii, and iii respectively represent PCL-KIO_3-100, PCL-KIO_3-150, and PCL-KIO_3-200 stent). The statistical analysis is performed by the one-way analysis of variance of Tukey's post-hoc test, $n = 6$, and $*$ indicates a significant difference of $p < 0.05$.

on a 3D-printed stent to evaluate cell proliferation (**Figure** 6A) and adhesion (Figure 6B). During the 7-day cell culture, all stents supported the adhesion and proliferation of HUVECs. The absorbance values of CCK-8 in PCL, PCL-KIO_3-100, and PCL-KIO_3-150 groups increased steadily, indicating that the introduction of a certain concentration of potassium iodate had no obvious side effect on the growth of HUVECs. After 1 day of culture, there was no significant difference in the number of HUVECs among the samples. After 4 and 7 days of culture, no significant difference was found in cell proliferation among PCL, PCL-KIO_3-100, and PCL-KIO_3-150 groups. Nevertheless, the number of HUVECs proliferating in the PCL-KIO_3-200 scaffold was lower than that in the other groups. Besides, HUVECs were observed on Calcein-AM stained stents after 4 and 7 days of culture. The results showed that the PCL, PCL-KIO_3-100, and PCL-KIO_3-150 group of cells grew and attached well. In comparison, the proliferation rate of HUVECs in the PCL-KIO_3-200 group decreased on Day 4. After 7 days of culture, the HUVECs adhered on the surface of the PCL-KIO_3-200 stent were less than that of other groups, which was consistent with the absorbance values of the CCK-8 assays. Moreover, the morphology of the cells on the surface of each group was observed by SEM (Figure 6C). At time points of 7 days, a large number of cell clusters adhered to PCL, PCL-KIO_3-100, and PCL-KIO_3-150 stents and the cells spread well, yet the cell adhesion on PCL-KIO_3-200 stent was inhibited. The analysis of cytocompatibility demonstrated that the addition of KIO_3 at certain concentrations supported the proliferation of HUVECs and the probability of endothelialization.

2.7. In Vivo Examination

For the evaluation in vivo, PCL-KIO_3 and PCL stents were implanted into the rabbit carotid artery (**Figure** 7A). Considering the cytocompatibility and visualization performance, PCL-KIO_3-150 stents were chosen as the PCL-KIO_3 groups. The angiography images of the stent status taken immediately after stent implantation and after 1, 3, and 6 months of post-implantation are shown in Figure 7B. The digital subtraction angiography (DSA) images showed the parent artery immediately after the PCL-KIO_3 stent was implanted. Under the interference of surrounding tissues, PCL stents were hard to investigate, while PCL-KIO_3 stents

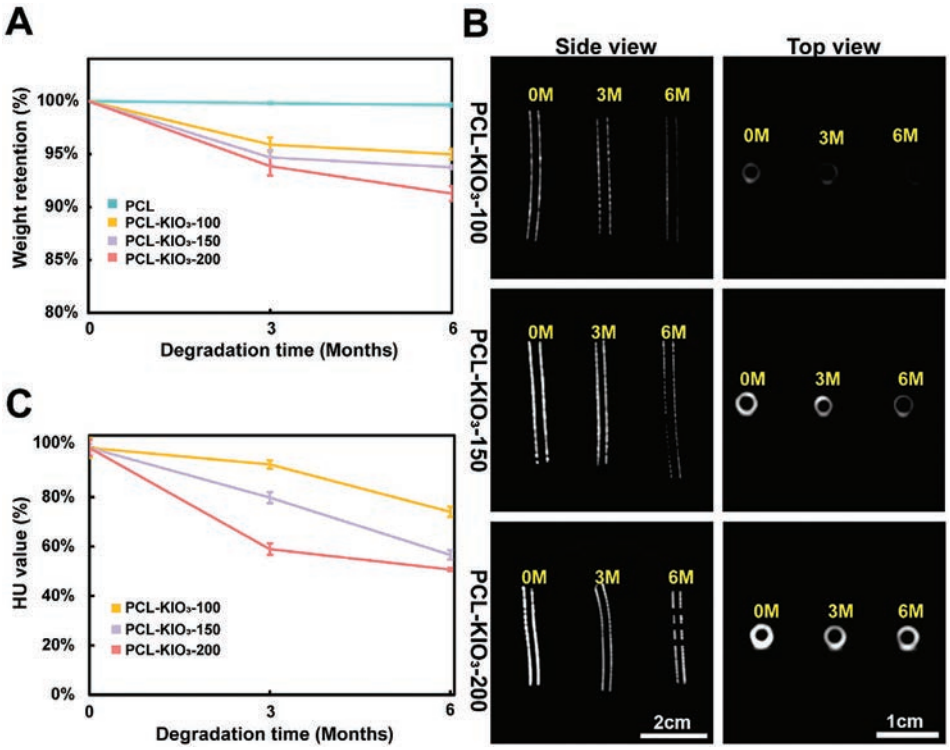

Figure 5. Degradation evaluation of stent in vitro environment. A) Weight retention fraction of PCL and PCL-KIO_3 stent during degradation. B) Representative radiographic images of PCL and PCL-KIO3 stent after 180 days of degradation which were placed in the air. C) The change of HU value of the PCL-KIO_3 stents after degradation.

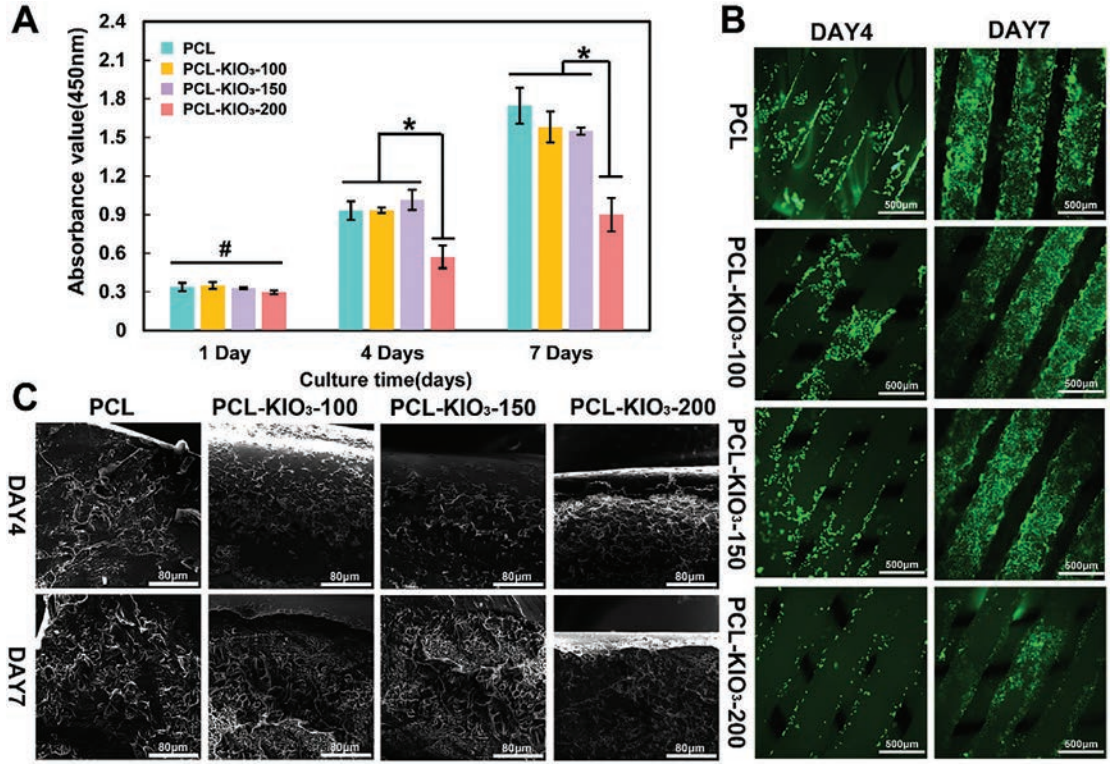

Figure 6. A) Proliferation of HUVECs on the surface of stents. B) Fluorescence microscopic morphology of HUVECs grown on the surface of stents after 4 and 7 days. C) SEM images of HUVECs cultured on stents after 4 and 7 days. The statistical analysis is performed by the one-way analysis of variance of Tukey's post-hoc test, $n = 3$, and $*$ indicates a significant difference of $p < 0.05$. # indicates no significant difference of $p > 0.05$.

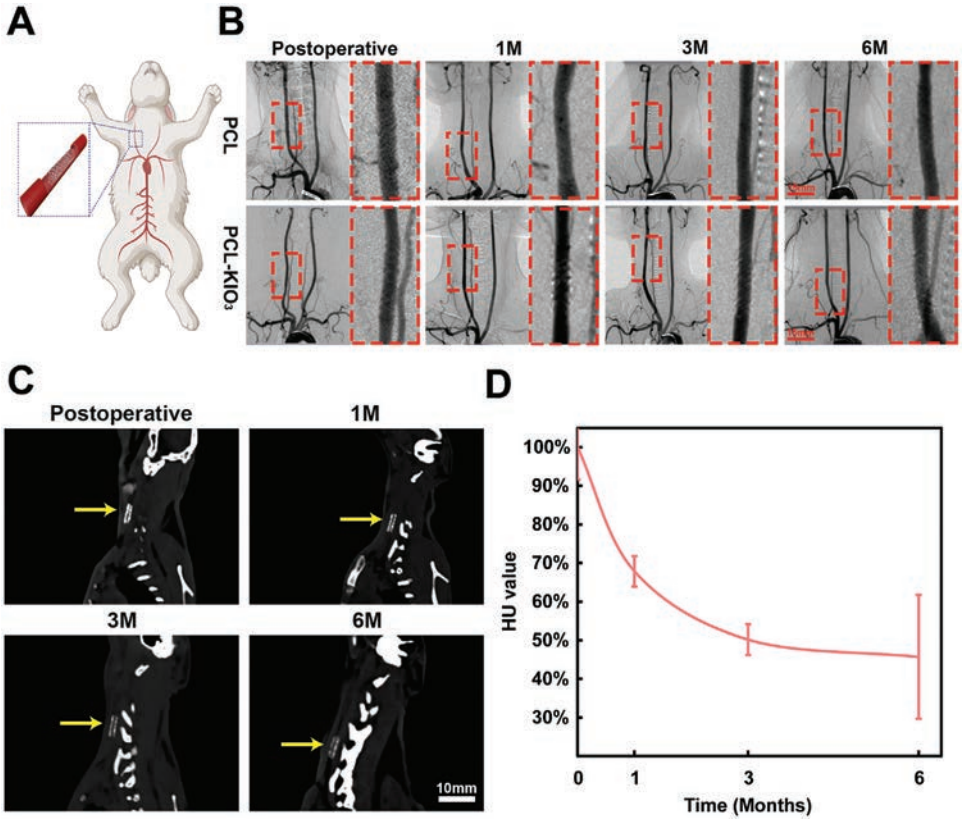

Figure 7. A) Schematic illustration for the stent deployment in rabbit carotid artery. B) Representative angiography images of PCL and PCL-KIO_3 stent implanted vessels after 1, 3, and 6 months of implantations. C) Representative CT reconstructed images of the PCL-KIO_3 stents after the implantation for 1, 3, and 6 months. The yellow arrow pointed to the PCL-KIO_3 stents. D) X-ray attenuation of intensity in Hounsfield units (HU) of the PCL-KIO_3 stents in vivo.

could be accurately positioned and tracked. During follow-up, PCL-KIO_3 stents could be observed in an X-ray bone window (Figure S4, Supporting Information). To further visualize the morphology of the radiopaque stent in vivo, the CT images were reconstructed. The PCL-KIO_3 stent could readily be visualized in the image, with sufficient density in contrast with the surrounding soft tissues via CT reconstruction (Figure 7C). Subsequently, corresponding time-dependent changes in the HU value of PCL-KIO_3 stents at 1, 3, and 6 months were respectively calculated (Figure 7D). The mean values of Hounsfield units of PCL-KIO_3 stents were 681.3, 462.3, 341.8, and 277.6 HU, respectively, for the post-operation, 1, 3, and 6 months.

For a comprehensive biological evaluation of the stents, all groups of stents were retrieved after 1, 3, and 6 months of implantation. Hematoxylin and eosin (H&E) staining demonstrated that both PCL stented vessels and PCL-KIO_3 stented vessels showed great patency within 6 months of implantation (**Figure** 8A). By calculation, the average neointimal area and the neointimal stenosis rate are shown in Figure 8B,C. The mean neointimal area was 0.66 ± 0.13 (1 month), 0.91 ± 0.22 (3 months), and 0.8 ± 0.14mm^2 (6 months) in the PCL stent group respectively, while 0.68 ± 0.13 (1 month), 0.86 ± 0.23 (3 months), and 0.69 ± 0.08mm^2 (6 months) in the PCL-KIO_3 stent group, respectively. Meanwhile, the neointimal stenosis rate was 20.87% (1 month), 27.21% (3 months), and 20.53% (6 months) in the PCL stent group, respectively, while 20.68% (1 month), 26.53% (3 months), and 23.78% (6 months) in the PCL-KIO_3 stent group, respectively. The introduction of KIO_3 may not increase the incidence of in-stent restenosis. Moreover, the platelet adhesion and the endothelial coverage were also evaluated through SEM. As shown in Figure 8D, endothelial cells gradually assemble on the surface of PCL and PCL-KIO_3 stents. No obvious thrombi were found in either group.

For optimal clinical use, it was essential to investigate the biosafety of radiopaque stents and in vivo pharmacokinetic profiles. The effects of KIO_3 released from PCL-KIO_3 stents on the histopathology of the kidney were examined by H&E staining (Figure S5, Supporting Information). No significant side effect was found in kidney tissue slices, indicating that the histopathological toxicity of KIO_3 release was puny. In addition, the serum levels of Total Triiodothyronine (TT3), Total Thyroxine (TT4), Free Triiodothyronine (FT3), and Free Thyroxine (FT4) were also evaluated (Figure S6, Supporting Information). The indices of TT3 and FT3 exhibited no significant change between the PCL group and the PCL-KIO_3 group. Due to the large release of KIO_3 at the initial implanting stage, the level of TT4 and FT4 in the PCL-KIO_3 group was higher than that of the PCL group at 1 month. At 3- and 6-months, the levels were restored to the same level as PCL groups. Moreover, the thyroid stimulating hormone (TSH) levels of PCL and PCL-KIO_3

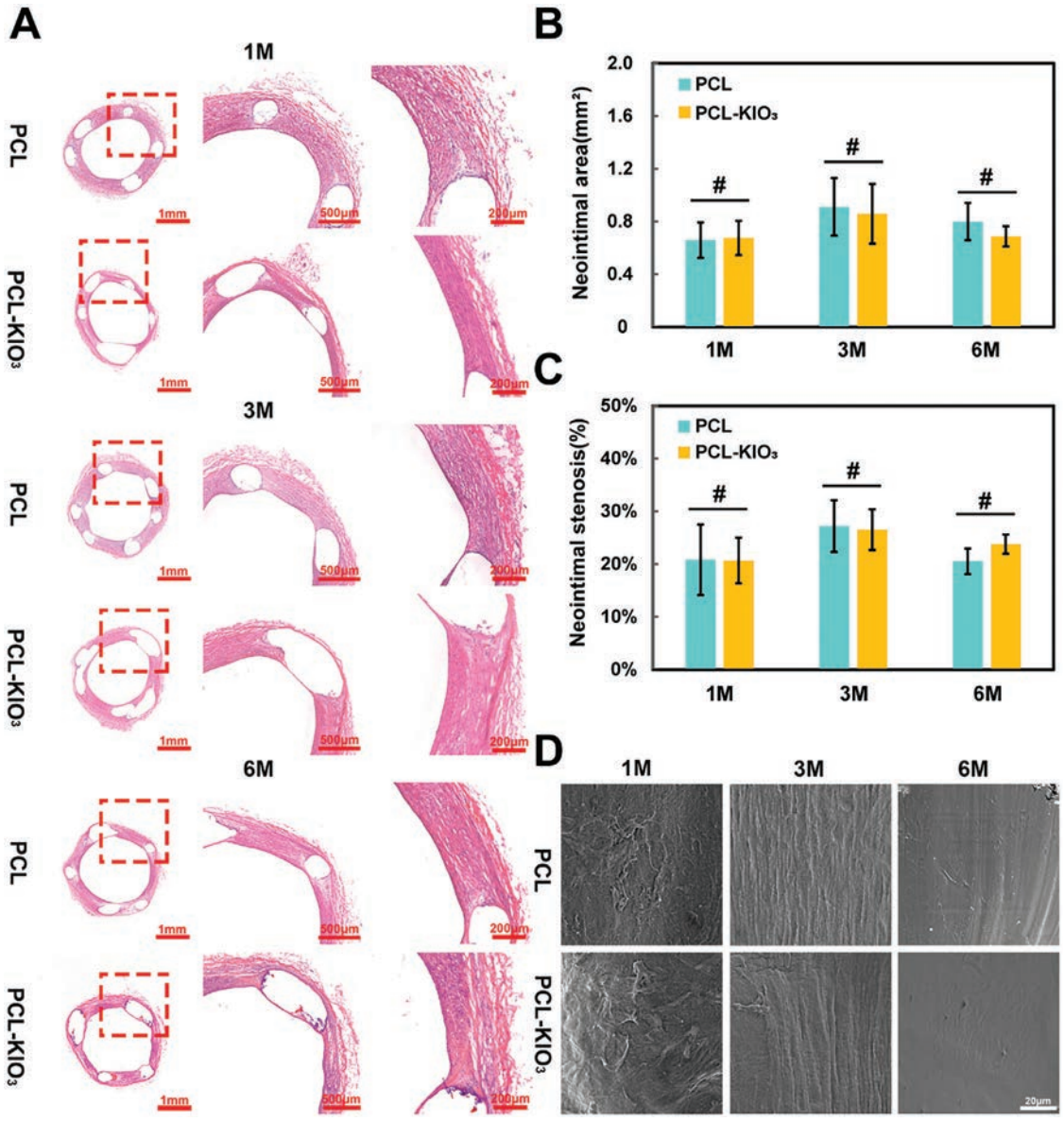

Figure 8. A) H&E staining images of PCL and PCL-KIO_3 stents implanted vessels during 6 months follow-up. B) Neointimal areas of stented vessels during 6 months follow-up, measured from H&E staining images. C) Neointimal stenosis of stented vessels during 6 months follow-up, measured from H&E staining images. D) SEM micrographs of the inner surface of the stents after PCL and PCL-KIO_3 stents were implanted for 1, 3, and 6 months. The statistical analysis is performed by unpaired Student's *t*-test, $n \geq 3$, and # indicates no significant difference of $p > 0.05$.

groups are below 0.05 mIU L^{-1} (Table S2, Supporting Information).

3. Discussion

EVT with a stent is considered an effective means for the treatment of cerebrovascular disease. Of note, biodegradable stents have attracted wide attention due to their degradability. The biodegradable stent can support stenotic arteries and recover normal blood supply to brain tissue and eventually absorbed by the body. In the process of stent implantation, the visualization of the stent is of great significance for stent deployment and follow-up. Stents need to be accurately delivered to the lesion site, so as to achieve the dilatation of stenotic vessels. In addition, the status of the stent dilatation is crucial to the success rate of EVT. Insufficient stent expansion may lead to thrombosis, while excessive stent expansion may burst the blood vessel. During the post-operative follow-up, whether the stent is displaced, fractured, or cracked needs to be tracked and observed.

The non-invasive imaging is a powerful tool for stent track during implantation and follow-up. X-ray imaging,[27] magnetic resonance imaging (MRI),[28,29] and fluorescence imaging[30] are widely used in the field of biomedical applications.[31] Among them, X-ray is one of the most available techniques for stent visualization in deep tissue. However, unlike metal stents, it is difficult to monitor biodegradable polymeric stents in

interventional therapy. Most polymers do not contain any elements with high electron density and high specific gravity. In order to enhance the X-ray contrast of polymeric stents, chemical modification and physical blending have been developed to achieve a robust method for the preparation of entirely X-ray visible stents. In comparison with chemical modification, the physical mixing process is stable and can be produced on an industrial scale because of its simple preparation process. Recently, various heavy metal particles, such as barium sulfate ($BaSO_4$), barium chloride, and iron oxide, have been tried to blend with polymers to improve the radiopacity of polymers. Ang et al.[32] have introduced $BaSO_4$ particles into poly (L-lactic acid) (PLLA) to prepare radiopaque biodegradable stents and realized the stent visualization in vitro. Similarly, Chang et al.[18] tried to combine BiOCl with poly (glycerol sebacate) acrylate (PGS), demonstrating the potential application of PGS-BiOCl in the monitoring of biodegradable medical implants in situ. Despite the fact that the intention of adding a heavy metal contrast agent in biodegradable polymer is to track the intactness of the stents, the application in vascular application is still unsatisfactory. The contrast agents, such as $BaSO_4$, are often used for gastrointestinal imaging, which can metabolize through the gastrointestinal tract and are not fit for intravascular imaging.[33,34] In addition, the potential toxicity of heavy metal particles is also a matter of concern. Instead of these metal particles, the non-metal compound potassium iodate can be a candidate with high radiopacity and excellent biocompatibility. In this study, we embedded the potassium iodate with PCL to prepare 3D-printed ink. Subsequently, the entirely X-ray visible stents were prepared via 3D printing. This strategy effectively combined iodinated contrast agents with biodegradable polymers to realize stent visualization.

As an iodine-containing compound, potassium iodate (KIO_3) is widely used for iodine supplementation in areas endemic to goiter.[35] KIO_3 contains the iodine atoms with high electron density, which endows the property of radiopacity. As expected, pure PCL was almost radiolucent and barely visible under X-ray. The introduction of KIO_3 had an influence on the improvement of the radiopacity of 3D-printed stents. The HU value of the PCL-KIO_3-150 stents could reach 389.67 HU. The radiographic images embedded in the pork could successfully verify the visibility of PCL-KIO_3 stents in deep tissue (Figure 4). These results laid the foundation for subsequent in vivo imaging. Moreover, the degradation of PCL-KIO_3 may exert an influence on long-term visualization. After 6 months of degradation, the outline of PCL-KIO_3-150 stents was still visible (Figure 5), which indicated the possibility of long-term follow-up application.

Although some radiopaque stents have been developed and the observation in vitro has been achieved, the visualization of the polymeric stents in vivo remains a severe challenge. Due to the increased background radiopacity resulting from bone and muscle tissue, the development effect of the X-ray visible stent implanted in the body may have a great negative impact, so that the status of the stent cannot be observed during the implantation or follow-up. In our study, the observation of PCL-KIO_3 stents in vivo was achieved by implanting into rabbit carotid artery (Figure 7). We observed that the PCL-KIO_3 stent was clearly visible at the moment of post-operation under DSA, which played an important role in helping the stent to be implanted into the rabbit carotid artery. After 6 months of implantation, the X-ray visible stent can still be tracked by DSA follow-up. The structural integrity of the stent was also evaluated by CT reconstruction. The structure of the stent was intact and a stent fracture did not appear. The radiopacity of the PCL-KIO_3 stent was reduced after 6 months. This may be attributed to the biodegradation of main PCL materials and the release of KIO_3. In terms of biodegradation, the in vitro degradation results demonstrated that the samples remained cylindrical shape and no significant changes occurred in their dimensions (Figure S1, Supporting Information). With the release of KIO_3 and the biodegradation, the mechanical properties of the stent may decrease. Due to the complexity of the vascular environment in vivo, biodegradable stents suffer from various mechanical loads after implantation, which exerts a great influence on the degradation profile.[36] According to the results of in vivo implantation, PCL-KIO_3 stents remained structural integrity for 6 months. The stability of the stent structure may be attributed to the slow degradation rate of PCL. Overall, the development of novel biodegradable and X-ray visible polymers may be helpful for long-term dynamic follow-up of the biodegradable stents.

In addition, the blood compatibility and biosafety of X-ray visible stents are key factors affecting surgical rate and vascular repair. The hemolysis rate test demonstrated that PCL-KIO_3 stents met the requirements of safe blood contact materials recommended by ISO10993-4. Compared with the PCL stent, there was no more platelet on the PCL-KIO_3 stent, indicating that the introduction of potassium iodate will not lead to more platelet adhesion (Figure S3A, Supporting Information). Angiography images also revealed that the blood vessels showed excellent patency after PCL and PCL-KIO_3 stent implantation (Figure 7A). In terms of biosafety, the proliferation of endothelial cells was evaluated. We observed that endothelial cells could stably survive on PCL-KIO_3-150 stents, indicating that the stents had low cytotoxicity (Figure 6). Moreover, the metabolism of contrast agents may have detrimental effects on tissues, which would limit the in vivo application of visible stents. Pathological results demonstrated that no evident differences were detected between the PCL and PCL-KIO_3 stents in kidney tissue slices (Figure S5, Supporting Information), thus indicating the KIO_3 can be normally metabolized through the kidney. Although the serum level of TT4 and FT4 transiently increased at 1 month, the levels were restored to the same level as PCL groups at 3 and 6 months. The PCL-KIO_3 stents would not cause permanent thyroid dysfunction (Figure S6, Supporting Information). Moreover, the TSH levels of PCL and PCL-KIO_3 groups are below 0.05 mIU L^{-1} (Table S2, Supporting Information). Overall, the issue with the biosafety of PCL-KIO_3 stents is acceptable.

Although these in vivo results are promising, the current study also has some limitations. Compared to the laser cutting technique, stents based on the 3D printing technique can be customized in accordance with the patient's vascular size and specific lesion environment. The cross-section of the printed stent strut is circular, while the laser-cutting stent strut is rectangular. Despite the unique advantage presented by 3D printing, their clinical applications have still suffered setbacks. Currently, the 3D-printed stent productions are largely confined to the preliminary laboratory-scale preparation stage. The precision and stability of fabricating stents are relatively insufficient. In addition, the strut thickness of the stents is still larger than metallic stents, which requires advanced 3D printing techniques and novel

design to optimize.[3] Moreover, the implantation period is not long enough for the observation of stent degradation in vivo. A longer-term follow-up is needed.

4. Conclusion

Based on physical blending and 3D printing, this study provided a robust method to develop an entirely X-ray visible stent. The imaging performance in vitro and in vivo and the biosafety after implanting in rabbit carotid artery were also evaluated. The results demonstrated that the introduction of potassium iodate endowed the biodegradable stents with X-ray radiopacity, which addressed the weakness of biodegradable polymeric stents in stent visualization. After 6 months of degradation in PBS solution, the PCL-KIO_3 stents containing a certain amount of potassium iodate could still be visualized under X-ray. Moreover, the addition of KIO_3 at a certain concentration would not lead to the adhesion of platelets or the inhibition of endothelial cells. The visualization in vivo, monitoring, and biocompatibility of PCL-KIO_3 stents were evaluated by implanting in the rabbit carotid artery. During the invasive stent deployment, the PCL-KIO_3 stent with radiopacity properties effectively helps us understand the position and dilation status of stents. At 6 months follow-up, the PCL-KIO_3 stents were still visible under X-ray. In addition, the stent showed good biocompatibility within 6 months and maintained great patency. These results confirmed the potential of 3D-printed biodegradable, entirely X-ray visible stents for application in cerebral vessels.

5. Experimental Section

Materials: PCL with molecular weight (MW) 80 kDa was purchased from Sigma-Aldrich Ltd (St. Louis, USA). Potassium iodate powder was purchased from Shanghai Macklin Biochemical Co., Ltd. The solvent DCM was from Sinopharm Chemical Reagents Co., Ltd. All reagents and polymer materials were used as received without purification.

Preparation of 3D-Printed Ink: The 3D-printed radiopaque ink was first prepared. 6 g PCL was added to 30 mL DCM solvent. The mixture was stirred overnight to obtain a homogeneous solution. Then, 0.6, 0.9, and 1.2 g potassium iodate powders were dissolved in the PCL solution. The PCL/KIO_3 solution evaporated slowly to obtain the PCL-KIO_3 composite. Finally, the PCL-KIO_3 composites were dried in a vacuum for 3 days to obtain the printed ink.

Fabrication of an Entirely X-ray Visible Cerebrovascular Stent: PCL-KIO_3 printed ink was utilized as the raw material for 3D printing. A homemade 4-axis printing system, consisting of a self-made rotary receiver and rapid prototyping manufacturing system (Bio-Architect SR; Regenovo Biotechnology Co., Ltd, China), was used to manufacture the X-ray visible stent. First, PCL-KIO_3 ink was added to the extrusion chamber and preheated to 140–150 °C for 20 min. The molten PCL-KIO_3 was extruded through the nozzle at the temperature of 160–165 °C. The nozzle point size was 1 mm. The extrusion nozzle moved at the speed of 2.5 mm s^{-1} along the center axis of the rotary receiver. The extrusion rate was 0.03 mm min^{-1}. Besides, the planar stents were prepared for relevant tests. The stents created with 100, 150, and 200 mg KIO_3/g PCL were identified as PCL-KIO_3-100, PCL-KIO_3-150, and PCL-KIO_3-200, respectively.

Characterization: The microstructure and morphology of PCL, PCL-KIO_3-100, PCL-KIO_3-150, and PCL-KIO_3-200 stents were observed by SEM (PhenomXL, Netherlands). Before scanning, a thin layer of gold-palladium was sputter coated on the samples via a sputter coater (SC7620, Quorum Technologies, USA). Then these samples were characterized by SEM at an accelerating voltage of 10 kV. The PCL-KIO_3 stent was characterized with an EDS (TM-1000, Hitachi, Japan) to observe the distribution of elements (C, O, I, and K). The XRD curves were evaluated on an X-ray diffractometer (AXS D8 Discover, Brukers, USA) within the scanning range of 2θ (10°–60°). The thermogravimetric analysis of PCL and PCL-KIO_3 stents was assessed in an inert atmosphere by using a thermogravimetric analyzer (Libra 209F1, Selb, Germany). The analysis was carried out at room temperature for up to 600 °C at a scan rate of 10 °C min^{-1}. To evaluate the release behavior of KIO_3, different PCL-KIO_3 groups were immersed in PBS (pH 7.4) at 37 °C. At the pre-determined time point, the solution was retrieved and an equal volume of the fresh media was added. The KI solution, starch indicator, and H_2SO_4 were respectively added to the retrieved media. The concentration of KIO_3 in each sample was determined by UV–vis at 580 nm. The apparent water contact angle analysis of PCL, PCL-KIO_3-100, PCL-KIO_3-150, and PCL-KIO_3-200 stents was carried out by using the contact angle analyzer (OCA40, Data-Physical, Germany) three times. 50 µL distilled water was dropped on the surface of the stents. The test system's software was then used to capture a photograph of the water droplets on the sample. The surface roughness of PCL and PCL-KIO_3 stents was measured using atomic force microscopy (AFM, MFP-3D, Germany).

Evaluation of the Visibility of Stents In Vitro: In order to evaluate the X-ray visibility of stents, X-ray equipment (SOMATOM FORCE, Siemens, Germany) for computed tomography (CT) was used. The scanning parameters were as follows: spatial resolution of 20 µm pixel size and scan thickness of 0.75 mm. For X-ray imaging in deep tissue, the lean pork at the thickness of 1 cm was put onto the PCL-KIO_3 stents layer by layer to evaluate X-ray visibility under deep tissue.

Mechanical Properties: The stent compression performance was performed in accordance with the standard ISO25539-2012 using a universal material testing machine (Instron-5542, Canton, USA) with a 200 N sensor (Transcell Technology, Inc., BAB-20MT, USA). PCL and PCL-KIO_3 stents were compressed to half of their original outer diameter. The compression load-displacement curve was recorded. The corresponding compression stress and compression modulus were calculated. Each stent was compressed for up to 50% of its deformation for ten cycles at a compression rate of 5 mm min^{-1} in loading–unloading fatigue tests. The compression cycle curve of the stent was obtained from the test. In accordance with the standard ASTM F2606-08, the three-point bending test was carried out. The following mechanical parameters were set: the length of the stent = 10 mm, the displacement rate = 0.1 mm min^{-1}, and the maximum displacement of the pressure device = 1.25 mm.

Evaluation of the Degradation of Stent In Vitro: The degradation of PCL and PCL-KIO_3 stents was performed in PBS solution (pH 7.4) at 37 °C in vitro. The stents were weighed (W_0) and immersed in PBS. The testing samples were shaken steadily on a horizontal shaker at 37 °C with a speed of 100 rpm. On monthly intervals for up to 6 months, testing samples were retrieved. Then, the samples were rinsed with deionized water. Afterward, the samples were freeze-dried and weighed again (W_t). The percentage of remaining mass was calculated as follows

$$\text{Percentage of remained mass } (\%) = W_t/W_0 \times 100\% \quad (1)$$

where W_0 and W_t, respectively, represent the weight of the samples at initial status and after degradation.

The morphology of stents after degradation was analyzed by SEM and the X-ray visibility of the stents at the pre-determined degradation time point was also evaluated.

Evaluation of the Hemocompatibility of Stents: In order to do the hemolysis test in vitro, a 2% (v/v) erythrocyte suspension was prepared by using New Zealand rabbit fresh whole blood. The erythrocyte solution was further diluted to a suspension (at a concentration of 2% (v/v)) after washing it with normal saline (NS) three times. Each sample was warmed in 10 mL of 37 °C saline for 30 min. 0.2 mL of erythrocyte suspension was respectively added to each sample. Afterward, in order to precipitate intact erythrocytes, all solutions were centrifuged at 3000 rpm after an hour of incubation at 37 °C. The optical density (OD) of samples was measured at 540 nm. Deionized water was chosen as the positive control and 0.9% NS as the negative control. After centrifugation at 1200 rpm, platelet-rich

plasma (PRP) supernatant was obtained from whole blood. The testing samples were incubated with 500 µL PRP for 2 h at 37 °C. Platelets adhered to the samples after incubation. Then, the unadhered platelet on the samples was removed by washing with warm PBS solution three times. After that, the testing sample was subsequently fixed with paraformaldehyde for 2 h, following rinsing with distilled water twice. The testing samples were then dehydrated by using a series of graded ethanol solutions (30, 50, 70, 80, 90, and 100%). The platelet morphology and platelet density were observed by SEM.

Cytocompatibility Assay: The planar stents of appropriate size (14 mm × 14 mm) were placed in a 24-well cell culture plate to evaluate the cell viability. After being secured by stainless steel rings, the planar PCL, PCL-KIO_3-100, PCL-KIO_3-150, and PCL-KIO_3-200 stent samples were washed with deionized water and sterilized with 75 vol% alcohol steam for 24 h. After irradiating with UV light for 12 h, PBS was used to wash the samples three times. The HUVECs suspension (3×10^4 cells/well) was seeded onto the surface of the stents and incubated at 37 °C, 5% CO_2 for up to 1, 4, and 7 days. At each time point, the medium was replaced with 200 µL of medium containing 10% CCK-8 reagent (Beyotime, China) and incubated for up to 2 h at 37 °C. Thereafter, the absorbance at 450 nm of supernatant was measured using a microplate reader (Multiskan MK3, Thermo, USA). For the assessment of the cell density, a live assay was performed by using a live cell staining kit (Yeasen Biotech, China). Briefly, HUVECs were seeded on the samples at the density of 3×10^4 cells/well. After 4 and 7 days of culture, PBS (200 µL) solution containing Calcein-AM was used instead of the cell culture medium. The fluorescence of cells was observed by a fluorescent microscope (DMi8, Leica, Germany). In terms of cell morphology, the testing sample was subsequently fixed with paraformaldehyde for 2 h. The testing samples were then dehydrated by using a series of graded ethanol solutions. The morphology of cells was observed by SEM.

In Vivo Assessments: All animal experiments were performed in accordance with the medical guidelines of Shanghai Jiao Tong University School for the housing and care of laboratory animals (Animal Welfare and Ethics Acceptance No. 2020-0524). The New Zealand white rabbits (3–5 months old, weight 2.5–3.3 kg,) were selected for PCL and PCL-KIO_3 stent implantation. Considering the potential side effects of PCL-KIO_3-200 stents, PCL-KIO_3-150 stents were chosen. A 2.5 × 15 mm stent was pressed into a 5.5-F catheter guide sheath beforehand after the ultraviolet sterilization process (30 min). After intramuscular injecting 1% sodium pentobarbital at 1 mg kg^{-1} and xylazine at 0.1 mg kg^{-1}, the rabbits were anesthetized. Animals were breathing spontaneously during surgery. The right groin skin of each rabbit was shaved and sterilized and a 6–8 cm incision was made. Thereafter, the femoral artery was then exposed and ruptured in order to insert a 6-F catheter sheath into the artery. A 6-F guiding catheter was inserted into the carotid artery's proximal segment in advance. The angiography revealed the patency of the carotid artery. The stent was fixed on the high compliance balloon (Emerge Monorail, Boston Scientific, US) by tying a temporary knot made of the biodegradable suture (5-0 Coated VICRYL, Cordis, US). Additionally, a surgical knot was used to secure the suture to the catheter close to the balloon. Under the guidance of the roadmap, the 3D printed stent-balloon system was advanced with the micro-guide wire guiding into the 5.5-F guiding catheter through the catheter guide sheath and eventually into the middle segment of the carotid artery. After delivering to the expected position (between the second cervical vertebra and the third cervical vertebra), a pressure pump was used to dilate the balloon to release the stent, and the temporary knot was released under the pressure of 8–12 kPa. The position and status of stents, as well as the patency of the carotid artery, can be observed through angiography. Eventually, the system was withdrawn. The incision was closed and the skin was sutured with 3–0 Vicryl. After the operation, enough food and water were fed to the animals, and heparin (400 U) was given intravenously for 3 days. 1 day before the operation and up to termination, all rabbits were fed with clopidogrel (7.5 mg) and aspirin (10 mg). During follow-up, DSA was performed to detect carotid artery patency and the structural integrity of implanted stents after 1, 3, and 6 months of implantation. The in vivo X-ray imaging properties of PCL-KIO_3 stents were evaluated by CT using multiplanar reformation. At the predetermined time intervals, an overdose intraperitoneal injection of isoprene barbiturate was used to sacrifice the rabbit. Afterward, the arteries containing the stents of the rabbits were retrieved. For histological analysis, cross-sections of stented vessels were stained with H&E. The mean neointimal area and neointimal stenosis rate were measured according to H&E staining. For biosafety studies, blood samples were collected for blood chemistry detection at predetermined time intervals. Then, the rabbits were sacrificed and the kidney tissues were harvested for histological examination.

Statistical Analysis: All the experiments were carried out at least in triplicate. The analysis of data was determined by unpaired Student's *t*-test or one-way analysis of variance of Tukey's post-hoc test. # indicates no significant difference of $p > 0.05$. ∗ indicates a significant difference of $p < 0.05$. All the statistical data were expressed as the mean ± standard deviation (SD). Data representations and statistical analyses were performed with Origin 9.1 software.

Supporting Information

Supporting Information is available from the Wiley Online Library or from the author.

Acknowledgements

Y.S. and C.T. contributed equally to this work. This work was supported by Science and Technology Commission of Shanghai Municipality, China (No. 20S31900900, 20DZ2254900) and Sino German Science Foundation Research Exchange Center, China (M-0263), China Education Association for International Exchange (2022181), Shanghai Pujiang Program (2020PJD043), Shanghai Science and Technology Innovation Project (201409006000); and The Foundation of MicroPort Medical Engineering (MP2021Q1C016). This project was also supported by Researchers Supporting Project Number (RSP2024R65), King Saud University, Riyadh, Saudi Arabia.

Conflict of Interest

The authors declare no conflict of interest.

Data Availability Statement

The data that support the findings of this study are available from the corresponding author upon reasonable request.

Keywords

3D printing, biodegradable stents, carotid artery, cerebrovascular disease, X-ray visible

Received: December 4, 2023
Revised: March 2, 2024
Published online: March 11, 2024

[1] J. Gutierrez, T. N. Turan, B. L. Hoh, M. I. Chimowitz, *Lancet Neurol.* **2022**, *21*, 355.
[2] M. Li, M. Jiang, Y. Gao, Y. Zheng, Z. Liu, C. Zhou, T. Huang, X. Gu, A. Li, J. Fang, *Bioact. Mater.* **2022**, *11*, 140.
[3] Y. Wang, G. Li, L. Yang, R. Luo, G. Guo, *Adv. Mater.* **2022**, *34*, 2201971.
[4] Y. Zhu, H. Zhang, Y. Zhang, H. Wu, L. Wei, G. Zhou, Y. Zhang, L. Deng, Y. Cheng, M. Li, H. Santos, W. Cui, *Adv. Mater.* **2019**, *31*, 1805452.
[5] Y. Shen, J. Cui, X. Yu, J. Song, P. Cai, W. Guo, Y. Zhao, J. Wu, H. Gu, B. Sun, X. Mo, *Smart Mater. Med.* **2024**, *5*, 36.
[6] Y. Shen, W. Zhang, Y. Xie, A. Li, X. Wang, X. Chen, Q. Liu, Q. Wang, G. Zhang, Q. Liu, J. Liu, D. Zhang, Z. Zhang, J. Ding, *Biomaterials* **2021**, *279*, 121208.

[7] D. Cao, J. Ding, *Regen. Biomater.* **2022**, *9*, rbac098.
[8] U. Sharma, D. Concagh, L. Core, Y. Kuang, C. You, Q. Pham, G. Zugates, R. Busold, S. Webber, J. Merlo, R. Langer, G. M. Whitesides, M. Palasis, *Nat. Mater.* **2018**, *17*, 96.
[9] H. Zhang, W. Zhang, H. Qiu, G. Zhang, X. Li, H. Qi, J. Guo, J. Qian, X. Shi, X. Gao, D. Shi, D. Zhang, R. Gao, J. Ding, *Adv. Healthcare Mater.* **2022**, *11*, 2201740.
[10] Y. Zhang, Q. Fang, *Medicine* **2020**, *99*, e20637.
[11] L. A. Dallan, V. N. Zimin, J. Lee, Y. Gharaibeh, J. N. Kim, G. T. Pereira, A. Vergara-Martel, P. Dong, L. Gu, D. L. Wilson, *Cardiovasc. Revasc. Med.* **2022**, *43*, 62.
[12] Y. Shen, X. Yu, J. Cui, F. Yu, M. Liu, Y. Chen, J. Wu, B. Sun, X. Mo, *Biomolecules* **2022**, *12*, 1245.
[13] J. P. Hytönen, J. Taavitsainen, S. Tarvainen, S. Ylä-Herttuala, *Cardiovasc. Res.* **2018**, *114*, 1063.
[14] E. Vahabli, J. Mann, B. S. Heidari, M. Lawrence-Brown, P. Norman, S. Jansen, E. De-Juan-Pardo, B. Doyle, *Adv. Healthcare Mater.* **2022**, *11*, e2200271.
[15] A. Karanasos, H. M. Garcia-Garcia, R.-J. van Geuns, E. Regar, *JACC: Cardiovasc. Interventions* **2015**, *8*, e53.
[16] T. R. Olsen, L. L. Davis, S. E. Nicolau, C. C. Duncan, D. C. Whitehead, B. A. Van Horn, F. Alexis, *Acta Biomater.* **2015**, *20*, 94.
[17] R. A. Hamideh, B. Akbari, P. Fathi, S. K. Misra, A. Sutrisno, F. Lam, D. Pan, *Adv. Healthcare Mater.* **2020**, *9*, e2000136.
[18] C.-T. Chang, H.-T. Chen, S. P. Girsang, Y.-M. Chen, D. Wan, S.-H. Shen, J. Wang, *Appl. Mater. Today* **2020**, *20*, 100771.
[19] Q. Wang, X. Yu, X. Chen, J. Gao, D. Shi, Y. Shen, J. Tang, J. He, A. Li, L. Yu, J. Ding, *ACS Appl. Mater. Interfaces* **2022**, *14*, 24197.
[20] C. Liu, H. Luo, M. Wan, L. Hou, X. Wang, Y. Shi, *Biomed. Mater. Eng.* **2018**, *29*, 269.
[21] V. Chausse, R. Schieber, Y. Raymond, B. Ségry, R. Sabaté, K. Kolandaivelu, M.-P. Ginebra, M. Pegueroles, *Addit. Manuf.* **2021**, *48*, 102392.
[22] K. Sneha, G. Sailaja, *J. Mater. Chem. B* **2021**, *9*, 8569.
[23] W.-J. Chang, Y.-H. Pan, J.-J. Tzeng, T.-L. Wu, T.-H. Fong, S.-W. Feng, H.-M. Huang, *PLoS One* **2015**, *10*, e0140354.
[24] A. Oskarsson, in *Handbook on the Toxicology of Metals*, Elsevier, New York **2022**, pp. 91–100.
[25] X. Ding, J. Zhu, A. Liu, Q. Guo, Q. Cao, Y. Xu, Y. Hua, Y. Yang, P. Li, *Tissue Eng. Regener. Med.* **2022**, *19*, 703.
[26] W. Krause, P. W. Schneider, in *Contrast Agents II: Optical, Ultrasound, X-Ray and Radiopharmaceutical Imaging*, (Ed: W. Krause), Springer Berlin Heidelberg, Berlin **2002**, pp. 107–150.
[27] F. Luderer, I. Begerow, W. Schmidt, H. Martin, N. Grabow, C. M. Bunger, W. Schareck, K. P. Schmitz, K. Sternberg, *J. Biomater. Appl.* **2013**, *28*, 219.
[28] H. Li, Y. Yin, Y. Xiang, H. Liu, R. Guo, *Biomed. Mater.* **2020**, *15*, 045004.
[29] J. Huang, Z. Lv, Y. Wang, Z. Wang, T. Gao, N. Zhang, M. Guo, H. Zou, P. Zhang, *Adv. Healthcare Mater.* **2016**, *5*, 2182.
[30] Y. Zhang, J. Yang, *J. Mater. Chem. B* **2013**, *1*, 132.
[31] M. F. Attia, B. R. Brummel, T. R. Lex, B. A. Van Horn, D. C. Whitehead, F. Alexis, *Adv. Healthcare Mater.* **2018**, *7*, 1800798.
[32] H. Y. Ang, D. Toong, W. S. Chow, W. Seisilya, W. Wu, P. Wong, S. S. Venkatraman, N. Foin, Y. Huang, *Sci. Rep.* **2018**, *8*, 17409.
[33] X. Yang, J. F. Lovell, Y. Zhang, *ChemBioChem* **2019**, *20*, 462.
[34] C. M. Oral, M. Ussia, M. Urso, J. Salat, A. Novobilsky, M. Stefanik, D. Ruzek, M. Pumera, *Adv. Healthcare Mater.* **2022**, *12*, 2202682.
[35] F. Delange, H. Bürgi, Z. P. Chen, J. T. Dunn, *Thyroid* **2002**, *12*, 915.
[36] Y. Li, Z. Chu, X. Li, X. Ding, M. Guo, H. Zhao, J. Yao, L. Wang, Q. Cai, Y. Fan, *Regen Biomater* **2017**, *4*, 179.